Numerical simulation of dripping and jetting in supercritical fluids/liquid micro coflows

Romain Guillaument, Arnaud Erriguible, Cyril Aymonier, Samuel Marre, Pascale Subra-Paternault

Numerical simulation of dripping and jetting in supercritical fluids/liquid micro coflows

Romain Guillaument [a], Arnaud Erriguible [a,*], Cyri Aymonier [b,c], Samue Marre [b,c,**], Pascale Subra-Paternault [d]

[a] Université de Bordeaux, Institut de Mécanique et d'Ingénierie – TREFLE, UMR CNRS 5295, 16 Avenue Pey Berland, 33607 Pessac Cedex, France
[b] CNRS, ICMCB, UPR9048, F-33600 Pessac, France
[c] Université de Bordeaux, ICMCB, UPR9048, F-33600 Pessac, France
[d] Université de Bordeaux, CBMN, CNRS UMR 5248, IPB, Allée Geoffroy St Hilaire, 33600 Pessac, France

Abstract

In this work, a two dimensional simulation of segmented micro coflows of CO_2 and water in micro-capillaries ($20 < T\,(^\circ C) < 50$ and $8 < p\,(MPa) < 16.5$) was carried out using a combination of the one-fluid model and the volume of fluid (VOF) method to describe the two-phase flow and a penalty method to account for the wetting property of the capillary walls. The computational work was validated by comparing numerical and experimental results in both the dripping and jetting regimes. The agreement of the calculated pressure difference across the droplet or jet interface with the Laplace–Young's law was assessed as supplementary criteria. The effects of CO_2/water interfacial tension ($5 < \sigma\,(mN\,m^{-1}) < 35$) and wall wettability (contact angle CO_2/wall varying from 0 to 180°) on the segmented water–supercritical CO_2 microflows were specially described. It was shown that switching the wall surface from hydrophilic to hydrophobic by tuning the contact angle allows for changing the droplet curvature so that the continuous water phase eventually undergoes a phase inversion resulting in water droplets/slugs formation in a continuous CO_2 phase.

1. Introduction

Over the past 15 years, the use of microfluidic devices in biology [1], chemistry [2] and materials science [3–5] has shown tremendous progresses. In particular, multiphase immiscible microflows have opened opportunities for generating controlled hydrodynamics structures (droplets, jets) allowing carrying out confined chemical reactions [4,6,7] or controlling reaction kinetics through reactivity at interfaces [8,9]. Droplets or jets are conventionally generated by mixing solutions through T-shape channel, flow focusing or coflow devices [10,11]. Recently, the design of microreactors withstanding high pressure and/or high temperature (typically up to 350 °C and 20 MPa) has driven the emergence of investigations with supercritical fluids [12–16], in which segmented or miscible flows can be created by manipulating flow rates or pressure. Supercritical fluids processes could largely benefit from the development of such microfluidic designs since droplets or jets are frequently encountered in materials synthesis or processing, like in the supercritical antisolvent process (SAS) [17–20] or in water–CO_2 microemulsions [21,22] for which the final materials characteristics are largely dependent on the initial hydrodynamic structures (size, polydispersity, *etc.*) [23,24]. Compared to macroscale approaches, the microfluidic generation and the subsequent confinement of such structures offer the opportunity to better control the droplets or jets uniformity, but also to perform *in situ* characterization [25], leading to advanced process mastering, as recently demonstrated for nanocrystals synthesis [26,27].

In microfluidics devices, the mechanisms of jets and droplets formation in both liquid–liquid and liquid–gas flows are largely studied [28,29]. The flow of immiscible fluids occurs generally in the form of segmented flow, where a disperse phase flowing in the center of the channel is segmented by a continuous liquid phase into distinct slugs. The continuous phase wets the wall so that the disperse elements are not in contact with the wall but fully surrounded by a liquid film. The transition from dripping to jetting and the droplets or jets size can be analytically determined by varying experimental parameters such as surface tension, viscosities and fluid velocities that are of peculiar importance in case of coflowing fluids [30,31]. Although these approaches are interesting for addressing the global behavior, numerical approaches [32] brings additional information such as velocity and pressure

* Corresponding author. Tel.: +33 540002700.
** Corresponding author at: CNRS, ICMCB, UPR9048, F-33600 Pessac, France.
E-mail addresses: erriguible@enscbp.fr (A. Erriguible), marre@icmcb-bordeaux.cnrs.fr (S. Marre).

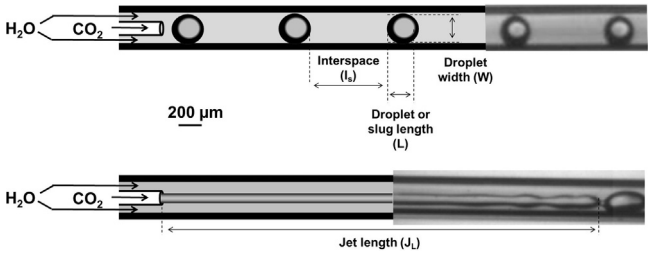

Fig. 1. Scheme of the general microcapillary-based coflowing configuration in the two regimes: (A) dripping or (B) jetting and additional relevant experimental and numerical geometrical parameters. The full set-up description can be found elsewhere [12].

gradient, profiles of surface tension and concentration that can be critical for the mixing of reagents as demonstrated for gas/liquid [33,34], liquid/liquid [35] microsystems or for supercritical/liquid macroscale process [36,37]. By predicting the flow behavior, simulations allow for reducing the experimental designs to the most valuable experiments.

The objective of this work is to develop a numerical approach for modeling the experimental observations of jets and drops generated by CO_2 and water micro coflows under high pressure conditions and high Reynolds numbers. This is a first step toward complete simulations of more complex processes, which could include various other physico-chemical phenomena (phase equilibria, chemical reactivity, nucleation and growth) occurring in real synthesis processes.

The first conditions simulated here correspond typically to the hydrodynamics encountered in a segmented microflow synthesis process. Then, the numerical approach is used to anticipate the effects of a given parameter on the flow characteristics. We focus on predicting the effect of interfacial forces on the flow, first by changing the surface tension – a parameter usually modified by adding surfactant to the fluid, and secondly by changing the wetting properties of the external capillary wall, which is more difficultly done by surface modifications, but which can occur as well during an experiment by the adhesion of reagents or synthetized particles with walls.

2. Experimental

2.1. Experimental set up

The capillary-based set-up was previously described elsewhere [12]. Briefly, the microsystem consisted of two silica capillaries inserted in one another. CO_2 and water were injected separately with high pressure syringe pumps (ISCO Teledyne 100 DM) generating a coflow (jet, drops or slugs) at the contacting point, as described in the general system configurations in both dripping and jetting regimes (Fig. 1). Pressure was controlled thanks to a back pressure regulator (JASCO BP2080) placed downstream the microsystem, while the entire set-up was immersed in a water bath for controlling temperature. Optical characterizations were performed with a high speed camera (Phantom V 9.1) connected to binocular microscope (Zeiss Stemi 2000-C). The inner diameters of internal and external capillaries were 100 and 250 μm, respectively (the external diameter of the internal capillary was 200 μm).

2.2. Determination of the relevant experimental parameters

The velocities at the desired operating conditions cannot be simply derived from the flow rates provided by the pumps since the fluids within the syringe reservoirs of the pumps are not at the same temperature than that of the microsystem, inducing density variations and therefore fluid expansions. In this work, conditions for the water and CO_2 reservoir were 25 °C and 0 °C, respectively, whereas the investigated conditions in the capillaries were in the range 20–80 °C. Thanks to the ISCO pumps running principle, the two fluids can be pressurized within the reservoir at the same pressure than the desired operating pressure, *e.g.* between 8 and 16.5 MPa. The fluids velocities within the microcapillaries, v_{int} for CO_2 and v_{ext} for water, were calculated as:

$$V_{\text{int}} = \frac{Q_{\text{int pump}}}{S_{\text{int}}} \times \frac{\rho_{\text{int}\,p,T_0}}{\rho_{\text{int}\,p,T}}, \quad V_{\text{ext}} = \frac{Q_{\text{extpump}}}{S_{\text{ext}}} \times \frac{\rho_{\text{ext}\,p,T_0}}{\rho_{\text{ext}\,p,T}}$$

with $Q_{\text{int pump}}$ and $Q_{\text{ext pump}}$ the pump flowrates for the internal and the external fluid, respectively, S_{int} and S_{ext} the inner section of the internal and external capillary, $\rho_{\text{int}\,p,T_0}$ and $\rho_{\text{ext}\,p,T_0}$ the density of the inner and outer fluid in the pump reservoir and $\rho_{\text{int}\,p,T_0}$ and $\rho_{\text{ext}\,p,T_0}$ the density of the inner and outer fluids at the experimental conditions.

The parameters required for the calculation of the relevant non dimensional numbers and used in the numerical modeling were either obtained from the NIST thermophysical properties online tools [38] (densities and viscosities for both $scCO_2$ and water at various pressure and temperature) or directly measured experimentally (interfacial tension for the $scCO_2$/water systems were determined from the pendant drop method).

The experimental errors on velocities are mostly related to the flowrates accuracy. For the ISCO 100 DM pumps used in this work, the flowrate uncertainty was estimated at $\pm 1\,\mu L\,min^{-1}$, which yielded to an experimental error of $\sim 1\,mm\,s^{-1}$ for velocity.

2.3. Microflows parameters

In this computational study, the numerical results were validated against experiments thanks to measurements provided by the images collected by the high speed camera (Fig. 1). The measured responses were:

- In case of dripping regime: the length (L) and width (W) of generated droplets or slugs and the interspace between droplets or slugs (I_s),
- In case of jetting regime: the jet length (J_L), and when droplets are formed by the jet breakup, their L, W and I_s.

The reported values were averaged from at least 50 pictures measurements. The uncertainty of L, W, I_s and J_L measurements came from the quality of the video collected during the experiments. Based on the pixel size and camera/binocular resolution and the averaged measurements, the overall error in a characteristic length was of ±20 μm.

3. Numerical section

Compressed CO_2 and water are the two fluids used in this work. In the range of investigated conditions, they are considered as immiscible fluids, so a two-phase flow has to be accounted for in the computational study. The two-phase flow was described by the one-fluid model [39] that was previously used for simulating a liquid jet breakup in pressurized CO_2 [37]. This one-fluid model considers each phase as fictitious domains that are merged into the global simulation domain. The boundary between the two fictitious domains was numerically tracked with an interface capturing method using a volume of fluid (VOF) approach [40]. This method has the advantage of being independent on the grid topology that is fixed and does not conform to the interface topology.

Table 1
Operating conditions of the three validation cases with additional numerical and experimental droplets/jets characteristic dimensions.

Case	v_{CO_2} (m s^{-1})	v_{Water} (m s^{-1})	T (°C)	P (MPa)	ρ_0 (CO_2) (kg m^{-3})	ρ_0 (H_2O) (kg m^{-3})	μ (CO_2) (μPa s)	μ (H_2O) (μPa s)	σ (mN m)	Experimental measurements (X μm ± 20 μm)				Numerical measurements (μm)			
										L	W	l_S	J_L	L	W	l_S	J_L
1	0.237 ± 0.01	0.094 ± 0.01	20	13	887	1004	88.5	1020	30	350	250	200	/	345	250	170	-
2	0.49 ± 0.01	0.65 ± 0.01	20	8	827	1001	75.7	998.4	30	250	250	590	/	250	250	400	-
3	0.146 ± 0.01	0.85 ± 0.01	50	16.5	731	995	60.8	549.9	7	160	160	630	730	160	160	700	700 ± 50

3.1. The one-fluid model

The one-fluid model considers a unique equivalent fluid whose physical properties are established with average or discontinuous properties of the flow built with the VOF color function C. This discontinuous or sharp varying function, defined for each phase as C_k, allows for localizing the phases in the computational domain. For a two phase flow, C_k admits two different values, 0 or 1, according to the phase it is associated with:

$$C_k(x,t) = \begin{cases} 1 & \text{if } x \in \Omega_k \\ 0 & \text{else} \end{cases} \tag{1}$$

where $k = 0, 1$ indicates the phase. From a Lagrangian point of view, the color function is advected by the interface velocity $\mathbf{u_I}$, which is the fluid velocity in our case since no phase change occurs. Therefore, C_k is the solution of an Eulerian advection equation:

$$\frac{\partial C_k}{\partial t} + \mathbf{u_I} \cdot \nabla C_k = 0 \tag{2}$$

The one-fluid model is obtained by the convolution of the Navier–Stokes equations in each phase with the color function and by summing in each equation the contribution of $k = 0$ and $k = 1$. The approach has already been described elsewhere [41]. Furthermore, the flow is considered as incompressible since the variation of pressure in the capillary is negligible so the pseudo-fluid equations read as:

$$\nabla \cdot \mathbf{u} = 0 \tag{3}$$

$$\rho\left(\frac{\partial \mathbf{u}}{\partial t} + \mathbf{u} \cdot \nabla \mathbf{u}\right) = -\nabla P + \rho \mathbf{g} + \nabla \cdot \mu[\nabla \mathbf{u} + \nabla^t \mathbf{u}] + \sigma \kappa \mathbf{n}_i \delta_i \tag{4}$$

$$\frac{\partial C}{\partial t} + \mathbf{u} \cdot \nabla C = 0 \tag{5}$$

This set of equations is similar to the Navier–Stokes equations set expressed for a single-phase flow, but with an additional advection equation of the color function C and a source term of surface tension force ($F_{st} = \sigma \kappa \mathbf{n}_i \delta_i$) in the momentum equation with κ the interface curvature, σ the interfacial tension between the two fluids, $\mathbf{n}_i$ the normal to the interface and δ_i the Dirac distribution at the interface.

The formulation of the one-fluid approach requires expressing all physical properties of the fluids as a function of the color function:

$$\begin{aligned} \rho &= \rho_0 + (\rho_1 - \rho_0)C \\ \mu &= \mu_0 + (\mu_1 - \mu_0)C \\ \kappa &= f_1(C) \\ \mathbf{n} &= f_2(C) \end{aligned} \tag{6}$$

These functions are used in the VOF methods to build the physical characteristics of the equivalent fluid at the interface vicinity. Since the single-fluid equations are not closed, it is necessary to also approximate the surface tension terms (curvature and normal to the interface) with appropriate functions dependent of C as described hereafter.

3.2. Numerical methods

The numerical methods, that are parts of the home-made CFD code Thétis developed at the I2M/TREFLE Department, have been already described and validated for a two-phase flow system at high pressure in case of Rayleigh breakup mechanism [37,41]. The one-fluid Navier–Stokes equations were discretized with implicit finite volumes on a staggered Cartesian grid. Centered or hybrid schemes

Table 2
Comparison between experimental and numerical results obtained for the three considered validation cases (blue: water, red: CO_2). Scale bar is 200 μm in all cases.

Case	Experimental	Numerical	Relative errors (%)			
			L	W	I_s	J_L
1		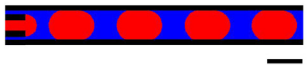	1.5	0	15	/
2	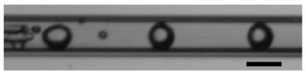	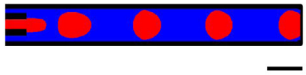	0	0	32	/
3		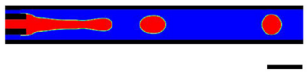	0	0	10	4

were implemented for discretizing all the numerical fluxes in the Navier–Stokes equations. The coupling between velocity and pressure was addressed with a projection method [42,43], solved by a BiCGSTAB II solver [44] preconditioned with a Jacobi method for the predictor step and an MCG approach (available in library HYPRE [44]) for the Poisson correction step. As for the interface tracking, the VOF approach was used with a piecewise linear interface construction (PLIC) [40]. This approach ensured the mass conservation while maintaining the interface width on one grid cell. The surface tension forces were approximated by the continuum surface force (CSF) approach of Brackbill [45]. In this case, the surface tension force reads to:

$$\begin{cases} \kappa = -\nabla \cdot \mathbf{n} = \nabla \cdot \left(\dfrac{\nabla C}{||\nabla C||} \right) \\ \mathbf{n}\delta_i = \nabla C \\ \sigma \kappa \mathbf{n} \delta_i = -\sigma \nabla \cdot \left(\dfrac{\nabla C}{||\nabla C||} \right) \nabla C \end{cases} \tag{7}$$

Wall wetting effects were emphasized as well in this work. The wetting property was imposed by a penalty method that allowed for varying the contact angle between the fluid and the capillary surface. The numerical method was detailed in Guillaument et al. [46,47]. A contact angle equal to 180° indicated that the surface was completely hydrophilic whereas the surface was completely hydrophobic for a contact angle of 0°.

Simulations were carried out in a 2D axi-symmetrical domain in order to reduce the computational time. The mesh sizes were of 85,680 (1260 × 68) to 342,720 (5040 × 68) nodes. Because of the high number of nodes, calculations were performed by MPI parallel programming.

4. Results and discussion

4.1. Validation

In order to validate the computational work and to prove its capability at representing various flow configurations, we confronted simulation and experimental results in conditions resulting in different hydrodynamic structures such as droplets, slugs and jets. Conditions and fluids properties are presented in Table 1, whereas Table 2 illustrates the experimental flows and the numerical results. Cases 1 and 2 correspond to high pressure liquid–liquid configuration whereas case 3 matches to a liquid–supercritical configuration. As criteria for validation, the various lengths detailed in Section 2.3 are reported in Table 1. Generally speaking, the transition in flow regime induced by these three conditions was well captured since droplets and jetting were clearly evidenced by simulations. The dimensions of the structures were also satisfactorily

Table 3
Validation of the Young's Laplace law in the three considered cases. An illustration of the numerical relative pressure field around one slug/droplet is displayed in each case.

Case	σ (mN/m)	r (μm)	Δp_{sim} (Pa)	ΔP_{th} (Pa)	Numerical relative pressure field around one droplet/slug	Relative Pressure scale (Pa)
1	30	133	460	451	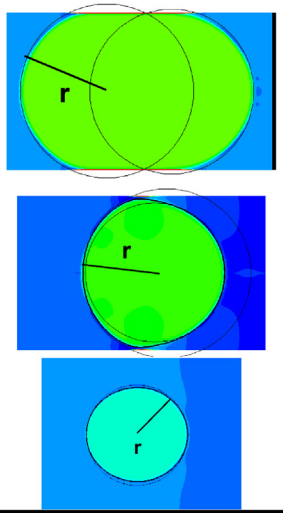	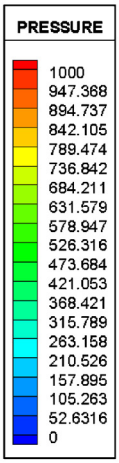
2	30	125	473	480		
3	7	82	172	171		

Table 4
Operating conditions of the five cases considered for investigating the surface tension effects over hydrodynamics (int = CO_2; ext = water). Please note that σ corresponds to the CO_2/water interfacial tension.

Case	T(°C)	P(MPa)	μ_{int}(μPa s)	μ_{ext}(μPa s)	ρ_{0int}(kg m^{-3})	ρ_{0ext}(kg m^{-3})	σ (mN/m)	v_{int}(m s^{-1})	v_{ext}(m s^{-1})	Re_{int}	Re_{ext}	We_{CO_2}	We_{water}	Ca_{CO_2}	Ca_{water}	Jet length (mm)
A	50	8	21.6	560	219	991	36	1.8	0.571	1825	51	1.971	0.4489	3	8.882	1.7
B	50	8	21.6	560	219	991	25	1.8	0.571	1825	51	2.838	0.6464	4	12.790	2.3
C	50	8	21.6	560	219	991	20	1.8	0.571	1825	51	3.548	0.8080	5	15.988	4
D	50	8	21.6	560	219	991	15	1.8	0.571	1825	51	4.730	1.0774	6	21.317	7.5
E	50	8	21.6	560	219	991	5	1.8	0.571	1825	51	14.191	3.2322	7	63.952	18.4

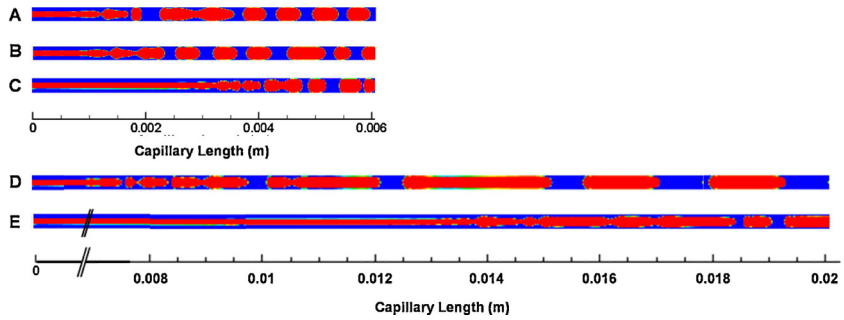

Fig. 2. Numerical color function fields (blue = water, red = CO_2) representing the effect of the CO_2/water interfacial tension (σ) over the jet length in the jetting regime. σ is: 36, 25, 20, 15 and 5 mN/m for case A, B, C, D and E, respectively. (For interpretation of the references to color in this figure legend, the reader is referred to the web version of this article.)

described since in the range of experimental uncertainties. The distance between the structures showed some deviation with the experience especially in case 2 where the interspace was underestimated by 32%. By looking closer at the capillary tip in the experimental picture, one can discern smaller satellite droplets in case 2, which formation can be induced by possible default in the alignment of capillaries resulting in "non-ideal" experimental flow.

In order to strengthen further the validation, the differential pressure across the droplet or slug interface was investigated.

The pressure difference across the interface between two fluids can be calculated with the Young–Laplace's law:

$$\Delta P_{th} = \sigma\left(\frac{1}{r_1} + \frac{1}{r_2}\right) \quad (8)$$

where r_1 and r_2 are the curvature radii in the characteristic planes of the local interfacial shape. By considering a spherical shape, we can assume that $r_1 = r_2 = r$. The Young–Laplace's law is highly important in physics since it comes from the phenomena of surface tension and relates the pressure difference to the shape of the surface. The good agreement between a simulated pressure difference and the Young Laplace's theoretical value would validate the formulation of the surface tension forces. For a given simulated droplet or slug as visualized in Table 3, the simulated and theoretical pressure differences were calculated. It can be first observed that the relative pressure is higher inside the droplets than outside. The deviations between simulated and theoretical values were below 4%, indicating that the capillary effects were well represented without parasitic currents by the surface tension formulation selected in this work. Hence, the proposed numerical scheme reproduced the different experimental configurations with a good confidence.

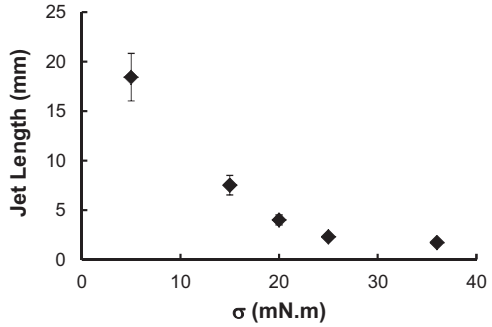

Fig. 3. Evolution of the jet length (J_L) as a function of the CO_2/water interfacial tension (σ) from the numerical simulation.

From this confirmation, the effects of surface tension and walls wettability on the hydrodynamics behavior of segmented water–supercritical CO_2 microflows were then investigated.

4.2. Effect of interfacial forces

4.2.1. Liquid–fluid surface tension

The influence of surface tension was investigated in liquid–supercritical configuration, *i.e.* in conditions of pressure above the critical pressure of CO_2 (p_c = 7.38 MPa, T_c = 31 °C). Five cases – whose conditions are summarized in Table 4 – were considered. Fluid velocities, fluids viscosities, pressure and temperature were kept constant whereas the water/supercritical CO_2 interfacial tension (σ) was tuned from 36 to 5 mN m^{-1}, which range is bounded by typical values of pure water–CO_2 systems [48] or water in presence of surfactants [49]. Fluid flows and especially multiphase flows exhibiting an interface between two immiscible fluids are characterized by several dimensionless numbers such as the Reynolds number ($Re = \rho v d/\mu$) describing the relative effect of inertial forces *versus* viscous forces, the Weber number ($We = \rho v 2d/\sigma$) that describes the relative importance of the fluid inertia compared to its surface tension and the capillary number ($Ca = \mu v/\sigma$) representing the comparative effect of viscous forces relative to the surface tension forces. A decrease of the surface tension hence impacts both on the Weber and the Capillary numbers (Table 4) so that inertial and viscous forces become dominant. Accordingly, the jet breakup changed as evidenced in Fig. 2. In the range of the surface tension investigated, the flow was always in the jetting regime, a behavior that fit the experimental evidences observed for liquid/liquid [29] and supercritical/liquid micro coflows [12] in case of Weber internal fluid and capillary external fluid numbers above 1. The jet length increased significantly as the surface tension decreased so that jets as long as 2 cm

Table 5
Operating conditions and corresponding physico-chemical parameters used for numerically studying the effect of wettability over the generated hydrodynamic structures.

v_{CO_2} (m s^{-1})	v_{Water} (m s^{-1})	T (°C)	P (MPa)	ρ_0 (CO_2) (kg m^{-3})	ρ_0 (H_2O) (kg m^{-3})	μ (CO_2) (μPa s)	μ (H_2O) (μPa s)	σ (mN m)
0.12	0.06	40	13	743	997	48	670	30

were obtained at small values of sigma (Fig. 3). This effect was equally observed experimentally.

It is worth noticing also the increase of the mean CO_2 slugs length (L) with a decreasing surface tension in the jetting regime (Fig. 2), although the inter-slugs distances (I_s) hardly change. This behavior could be the expression of an increasing wavelength of the convective instability with perturbations that propagate downstream while growing.

4.2.2. Surface wettability

Wetting properties of the wall can affect drastically the flow hydrodynamics [50,51] and consequently the particle transport in case of material synthesis [52]. Experimentally, the wetting depends of the surface chemistry, surface quality and/or contamination. Several experimental means are available from the literature for purposefully modifying surface contact angle, including silanes covalent bonding through self assembly monolayer (SAM) [53], surface adsorption of molecules such as surfactants or surface nanostructuration [54]. However, it is still somewhat difficult to achieve a perfect control of the contact angle, resulting in a need for modeling. The present model allows for taking into account the wetting properties by means of the contact angle between the CO_2 phase and the walls. In the previous configurations, we have considered that the surface was hydrophilic due to the silica nature of the capillaries and consequently the wall was completely wet by the external water (contact angle: $\alpha = 180°$). In this sub-section, the contact angle was tuned from $\alpha = 180°$ (which could characterize a hydrophilic surface) down to $\alpha = 0°$, which characterizes a hydrophobic coating. Between these extrema cases of hydrophobicity, intermediary situations can be created for instance by surface roughness or inhomogeneous coating. Conditions of simulations are reported in Table 5 and the simulated flows are shown in Fig. 4.

A remarkable result is that the contact angle, and thus, the wettability provokes the inversion of the emulsion, *e.g.* although the CO_2 is still injected at the center of the water flow, the water minimizes its interaction with the hydrophobic wall and rearranges itself as droplets or slugs now separated by interspaces of CO_2 wetting the wall (see in particular the simulations at $\alpha = 160°$ and $\alpha = 40°$). This is similar to a former study by Kuhn et al. [55] in which the impact of Teflon-modified silicon surface on a toluene–water flow

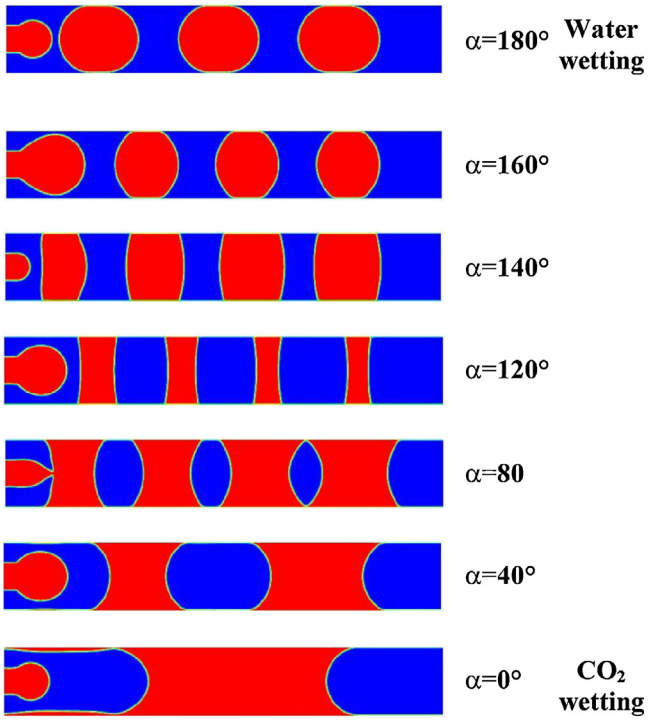

Fig. 4. Numerical color function fields (blue = water, red = CO_2) representing the effect of the CO_2/wall contact angle (α) over the droplets/slugs shapes ($T = 40$ °C, $p = 13$ MPa, v_{int} (CO_2) = 0.12 m s^{-1} and v_{ext} (water) = 0.06 m s^{-1}). (For interpretation of the references to color in this figure legend, the reader is referred to the web version of this article.)

was experimentally investigated. By first modifying silica surface with fluorosilanes and further depositing Teflon onto the walls, the surface was switched from hydrophilic to hydrophobic. Consequently, toluene wets the wall and the initial continuous water phase is isolated in droplets. Between those extreme situations, the contact angle affected the droplet shape and size, which is consistent for instance with the meniscus deformation observed when varying the number of hydrophobic surfaces of a microchannel [56]. At large values, the increasing hydrophobicity (decreasing contact

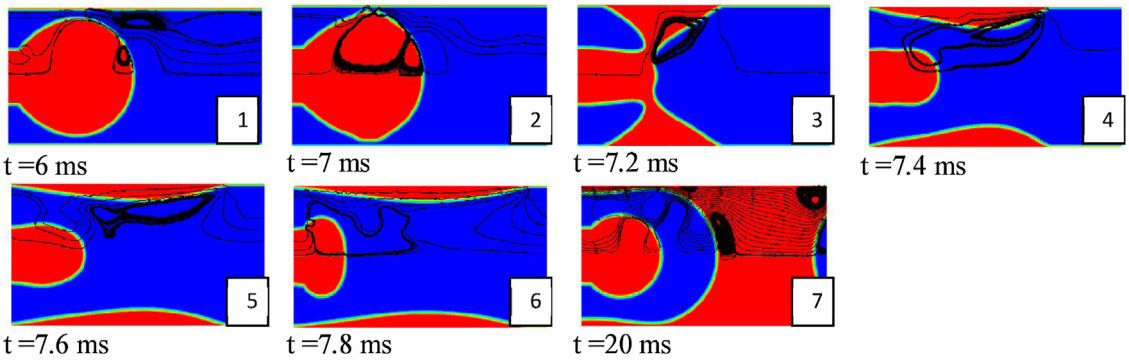

Fig. 5. Various time snapshots of the phase inversion mechanism (blue = water, red = CO_2). These pictures are combined in a movie, which can be found in the supporting information for better mechanism visualization ($T = 40$ °C, $p = 13$ MPa, v_{int} (CO_2) = 0.12 m s^{-1} and v_{ext} (water) = 0.06 m s^{-1}, $\alpha = 0°$). (For interpretation of the references to color in this figure legend, the reader is referred to the web version of this article.)

angle) provokes the acceleration of droplets due to the decrease of the adhesion at the wall surface and generates therefore the deformation of the slug. Below the critical value of 120°, the wall surface became more wet by carbon dioxide so that a phase switching occurred.

A closer look at the mechanism responsible of this particular phenomena is given in Fig. 5 that reports both streamlines, which show the presence of vortex near the interfaces due to interfacial tension phenomena and the evolution of the color function for different times near the injector. As a first step, the volume of the CO_2 droplet created at the vicinity of the inner capillary tip increases (Images 1–2). When this drop comes into contact with the wall that has affinity for CO_2, the droplet is destructured resulting in CO_2 segments sliding on the wall (Images 3–4) and displacing water toward the center of the channel (Images 4–6). When the CO_2 accumulation is sufficient at the wall, the capillary effects create a bridge between the two walls (Image 7) so that a periodic CO_2 bridge is formed and segments the water phase in droplets (see also the movie in the supporting information). Since the wall becomes covered by CO_2, the water droplets are isolated from each other and do not communicate anymore.

Supplementary data related to this article found, in the online version, at http://dx.doi.org/10.1016/j.supflu.2013.04.011.

5. Conclusion

In this work, a simulation approach of supercritical fluid–liquid micro coflows was proposed in the context of material synthesis in microreactors with a special insight at the effect of capillary forces on the phase behavior. Accordingly, a two-phase flow was simulated in 2D using the one-fluid model combined to the volume-of-fluid (VOF) approach to track the interface. The simulated flows were compared to experimental observations performed in a capillary-based coflowing microreactor with images recorded with a high speed camera. Good agreements were obtained between simulated and experimental microflows characteristics (droplet or jet size, interspace between droplets), which enabled to numerically study the effect of surface tension and wettability with reasonable confidence. In the jetting regime, the decrease of surface tension led to a significant increase of the jet length. Considering the dripping regime, the surface wettability was varied numerically from hydrophilic to hydrophobic *via* contact angle variation, resulting in an evolution from CO_2 droplets in a water continuous phase to water droplets in a CO_2 continuous phase. In particular, the results demonstrated the strong effect of small variations of the contact angle over the final hydrodynamics structures shape. The results obtained in the frame of this study can be used to anticipate effects that can be purposefully mastered to control the formation of micro volumes in supercritical process. Additionally, these allow getting toward more complex process simulation by later including heat and mass transfer, chemical reactions and/or nucleation/growth mechanisms used in various fields of research, both at macro- and microscale.

Acknowledgments

Authors thank the Aquitaine Regional Council for the financial investment in a 256-processor cluster located at I2M TREFLE Department and through the Advanced Materials in Aquitaine funding. Computer time was also provided by the computing facilities MCIA (Mésocentre de Calcul Intensif Aquitain) of the Bordeaux and Pau et des Pays de l'Adour Universities. The Agence Nationale pour la Recherche (ANR) is also gratefully acknowledged for funding the CGSμLab project.

References

[1] C. Hansen, S.R. Quake, Microfluidics in structural biology: smaller, faster... better, Current Opinion in Structural Biology 13 (5) (2003) 538–544.
[2] R.L. Hartman, K.F. Jensen, Microchemical systems for continuous-flow synthesis, Lab on a Chip – Miniaturisation for Chemistry and Biology 9 (17) (2009) 2495–2507.
[3] S. Marre, K.F. Jensen, Synthesis of micro and nanostructures in microfluidic systems, Chemical Society Reviews 39 (3) (2010) 1183–1202.
[4] A.M. Nightingale, S.H. Krishnadasan, D. Berhanu, X. Niu, C. Drury, R. McIntyre, J.C. Demello, A stable droplet reactor for high temperature nanocrystalsynthesis, Lab on a Chip – Miniaturisation for Chemistry and Biology 11 (7) (2011) 1221–1227.
[5] J.I. Park, A. Saffari, S. Kumar, A. Günther, E. Kumacheva, Microfluidic synthesis of polymer and inorganic particulate materials, Annual Review of Materials Research 40 (2010) 415–443.
[6] T. Noël, J.R. Naber, R.L. Hartman, J.P. Mcmullen, K.F. Jensen, S.L. Buchwald, Palladium-catalyzed amination reactions in flow: overcoming the challenges of clogging via acoustic irradiation, Chemical Science 2 (2) (2011) 287–290.
[7] N. Lorber, F. Sarrazin, P. Guillot, P. Panizza, A. Colin, B. Pavageau, E. Mignard, Some recent advances in the design and the use of miniaturized droplet-based continuous process: applications in chemistry and high-pressure microflows, Lab on a Chip – Miniaturisation for Chemistry and Biology 11 (5) (2011) 779–787.
[8] H. Song, D.L. Chen, R.F. Ismagilov, Reactions in droplets in microflulidic channels, Angewandte Chemie – International Edition 45 (44) (2006) 7336–7356.
[9] R. Seemann, M. Brinkmann, T. Pfohl, S. Herminghaus, Droplet based microfluidics, Reports on Progress in Physics 75 (1) (2012).
[10] S-Y. Teh, R. Lin, L-H. Hung, A-P. Lee, Droplet Microfluidics, Lab on a Chip 8 (2) (2008) 198–220.
[11] D.M. Fries, S. Waelchli, P. Rudolf von Rohr, Gas–liquid two-phase flow in meandering microchannels, Chemical Engineering Journal 135 (Suppl. 1) (2007) S37–S45.
[12] S. Marre, C. Aymonier, P. Subra, E. Mignard, Dripping to jetting transitions observed from supercritical fluid in liquid microcoflows, Applied Physics Letters 95 (13) (2009).
[13] J. Keybl, K.F. Jensen, Microreactor system for high-pressure continuous flow homogeneous catalysis measurements, Industrial and Engineering Chemistry Research 50 (19) (2011) 11013–11022.
[14] S. Marre, Y. Roig, C. Aymonier, Supercritical microfluidics: opportunities in flow-through chemistry and materials science, Journal of Supercritical Fluids 66 (2012) 251–264.
[15] S. Marre, A. Adamo, S. Basak, C. Aymonier, K.F. Jensen, Design and packaging of microreactors for high pressure and high temperature applications, Industrial and Engineering Chemistry Research 49 (22) (2010) 11310–11320.
[16] E. Carretier, E. Badens, P. Guichardon, O. Boutin, G. Charbit, Hydrodynamics of supercritical antisolvent precipitation: characterization and influence on particle morphology, Industrial and Engineering Chemistry Research 42 (2) (2003) 331–338.
[17] F. Trachsel, B. Tidona, S. Desportes, P. Rudolf von Rohr, Solid catalyzed hydrogenation in a Si/glass microreactor using supercritical CO_2 as the reaction solvent, Journal of Supercritical Fluids 48 (2) (2009) 146–153.
[18] E. Reverchon, E. Torino, S. Dowy, A. Braeuer, A. Leipertz, Interactions of phase equilibria, jet fluid dynamics and mass transfer during supercritical antisolvent micronization, Chemical Engineering Journal 156 (2) (2010) 446–458.
[19] A. Tenorio, P. Jaeger, M.D. Gordillo, C.M. Pereyra, E.J.M. De La Ossa, On the selection of limiting hydrodynamic conditions for the supercritical AntiSolvent (SAS) process, Industrial and Engineering Chemistry Research 48 (20) (2009) 9224–9232.
[20] C. Roy, D. Vrel, A. Vega-González, P. Jestin, S. Laugier, P. Subra-Paternault, Effect of CO_2-antisolvent techniques on size distribution and crystal lattice of theophylline, Journal of Supercritical Fluids 57 (3) (2011) 267–277.
[21] S.S. Adkins, X. Chen, I. Chan, E. Torino, Q.P. Nguyen, A.W. Sanders, K.P. Johnston, Morphology and stability of CO_2-in-water foams with nonionic hydrocarbon surfactants, Langmuir 26 (8) (2010) 5335–5348.
[22] J.L. Dickson, P.A. Psathas, B. Salinas, C. Ortiz-Estrada, G. Luna-Barcenas, H.S. Hwang, K.P. Johnston, Formation and growth of water-in-CO_2 miniemulsions, Langmuir 19 (12) (2003) 4895–4904.
[23] D.L. Obrzut, P.W. Bell, C.B. Roberts, S.R. Duke, Effect of process conditions on the spray characteristics of a PLA + methylene chloride solution in the supercritical antisolvent precipitation process, Journal of Supercritical Fluids 42 (2) (2007) 299–309.
[24] K.T. Lim, H.S. Hwang, M.S. Lee, G.D. Lee, S.S. Hong, K.P. Johnston, Formation of TiO_2 nanoparticles in water-in-CO_2 microemulsions, Chemical Communications 14 (2002) 1528–1529.
[25] A. Ahmadi, K.D. Devlin, H. Najjaran, J.F. Holzman, M. Hoorfar, In situ characterization of microdroplet interfacial properties in digital microfluidic systems, Lab on a Chip – Miniaturisation for Chemistry and Biology 10 (11) (2010) 1429–1435.
[26] Y. Roig, S. Marre, T. Cardinal, C. Aymonier, Synthesis of exciton luminescent ZnO nanocrystals using continuous supercritical microfluidics, AngewandteChemie – International Edition 50 (50) (2011) 12071–12074.
[27] T. Gendrineau, S. Marre, M. Vaultier, M. Pucheault, C. Aymonier, Microfluidic synthesis of palladium nanocrystals assisted by supercritical CO_2: tailored

surface properties for applications in boron chemistry, AngewandteChemie – International Edition 51 (34) (2012) 8525–8528.
[28] A.S. Utada, L. Chu, A. Fernandez-Nieves, D.R. Link, C. Holtze, D.A. Weitz, Dripping, jetting, drops, and wetting: the magic of microfluidics, MRS Bulletin 32 (9) (2007) 702–708.
[29] T.M. Keenan, C. Hsu, A. Folch, Microfluidic jets for generating steady-state gradients of soluble molecules on open surfaces, Applied Physics Letters 89 (11) (2006).
[30] P. Guillot, A. Colin, A. Ajdari, Stability of a jet in confined pressure-driven biphasic flows at low Reynolds number in various geometries, Physical Review E – Statistical, Nonlinear, and Soft Matter Physics 78 (1) (2008).
[31] M.A. Herrada, A.M. Gañán-Calvo, A. Ojeda-Monge, B. Bluth, P. Riesco-Chueca, Liquid flow focused by a gas: jetting, dripping, and recirculation, Physical Review E – Statistical, Nonlinear, and Soft Matter Physics 78 (3) (2008).
[32] R. Gupta, D.F. Fletcher, B.S. Haynes, On the CFD modelling of taylor flow in microchannels, Chemical Engineering Science 64 (12) (2009) 2941–2950.
[33] M. Wörner, Numerical modeling of multiphase flows in microfluidics and micro process engineering: a review of methods and applications, Microfluidics and Nanofluidics 12 (6) (2012) 841–886.
[34] T. Taha, Z.F. Cui, CFD modelling of slug flow inside square capillaries, Chemical Engineering Science 61 (2) (2006) 665–675.
[35] R. Raj, N. Mathur, V.V. Buwa, Numerical simulations of liquid–liquid flows in microchannels, Industrial and Engineering Chemistry Research 49 (21) (2010) 10606–10614.
[36] A. Martín, M.J. Cocero, Numerical modeling of jet hydrodynamics, mass transfer, and crystallization kinetics in the supercritical antisolvent (SAS) process, Journal of Supercritical Fluids 32 (1–3) (2004) 203–219.
[37] A. Erriguible, S. Vincent, P. Subra-Paternault, Numerical investigations of liquid jet breakup in pressurized carbon dioxide: conditions of two-phase flow in supercritical antisolvent process, Journal of Supercritical Fluids 63 (2012) 16–24.
[38] NIST, Thermophysical Properties of Pure Fluids Database NIST12, NIST, Gaithersburg, MD, 2000.
[39] I. Kataoka, Local instant formulation of two-phase flow, International Journal of Multiphase Flow 12 (5) (1986) 745–758.
[40] D.L. Youngs, Time-dependent multi-material flow with large fluid distortion, in: K.W. Morton, M.J. Baines (Eds.), Numerical Methods for Fluid Dynamics, Academic Press, New York, 1982.
[41] J. Delteil, S. Vincent, A. Erriguible, P. Subra-Paternault, Numerical investigations in rayleigh breakup of round liquid jets with VOF methods, Computers and Fluids 50 (1) (2011) 10–23.
[42] K. Goda, A multistep technique with implicit difference schemes for calculating two- or three-dimensional cavity flows, Journal of Computational Physics 30 (1) (1979) 76–95.
[43] E. Ahusborde, S. Glockner, An implicit method for the Navier-Stokes equations on overlapping block-structured grids, International Journal for Numerical Methods in Fluids 62 (7) (2010) 784–801.
[44] R.D. Falgout, U.M. Yang, Hypre: a library of high performance preconditioners, in: P.M.A. Sloot, C.J.K. Tan, J.J. Dongarra, A.G. Hoekstra (Eds.), Lecture Notes in Computer Science, 2331, Springer-Verlag, Berlin, Heidelberg, 2002, pp. 632–664, Computational Science-CARS 2002 Part III.
[45] J.U. Brackbill, A continuum method for modeling surface tension, Journal of Computational Physics 100 (2) (1992) 335–354.
[46] R. Guillaument, S. Vincent, J.P. Caltagirone, M. Laugier, P. Gardin, Plate-out modelling for cold rolling system lubricated with o/w emulsion, in: Proceedings of IMechE, vol. 225 Part J: Journal of Engineering Tribology, 2011.
[47] R. Guillaument, Modélisation globale de l'alimentation d'une emprise lubrifiée par émulsion: simulation numérique directe et analyse physique des phénomènes, de l'Université Bordeaux 1, 2010 (Thèse de doctorat).
[48] E. Badens, O. Boutin, G. Charbit, Laminar jet dispersion and jet atomization in pressurized carbon dioxide, Journal of Supercritical Fluids 36 (1) (2005) 81–90.
[49] M. Sagisaka, T. Fujii, Y. Ozaki, S. Yoda, Y. Takebayashi, Y. Kondo, K. Otake, Interfacial properties of branch-tailed fluorinated surfactants yielding a water/supercritical CO_2 microemulsion, Langmuir 20 (7) (2004) 2560–2566.
[50] S.C. Yang, Effects of surface roughness and interface wettability on nanoscale flow in a nanochannel, Microfluidics and Nanofluidics 2 (6) (2006) 501–511.
[51] N. Shao, A. Gavriilidis, P. Angeli, Flow regimes for adiabatic gas-liquid flow in microchannels, Chemical Engineering Science 64 (11) (2009) 2749–2761.
[52] M.-Y. Zhou, R. Xie, Y.-L. Yu, G. Chen, X.-J. Ju, L. Yang, B. Liang, L.-Y. Chu, Effects of surface wettability and roughness of microchannel on flow behaviors of thermo-responsive microspheres therein during the phase transition, Journal of Colloid and Interface Science 336 (2009) 162–170.
[53] U. Srinivasan, M.R. Houston, R.T. Howe, R. Maboudian, Alkyltrichlorosilanebased self-assembled monolayer films for stiction reduction in silicon micromachines, Journal of Microelectromechanical Systems 7 (1998) 252–260.
[54] J. Zhou, D.A. Khodakov, A.V. Ellis, N.H. Voelcker, Surface modification for PDMS-based microfluidic devices, Electrophoresis 33 (2012) 89–104.
[55] S. Kuhn, R.L. Hartman, M. Sultana, K.D. Nagy, S. Marre, K.F. Jensen, Teflon-coated silicon microreactors: impact on segmented liquid–liquid multiphase flows, Langmuir 27 (10) (2011) 6519–6527.
[56] S. Sultana, J. Matsui, M. Mitsuishi, T. Miyashita, Flow behavior in surface-modified microchannels with polymer nanosheets, Thin Solid Films 518 (2) (2009) 606–609.